Spontaneous exchange bias effect in polycrystalline Bi 0.5 Sr 0.5 Fe 0.5 Cr 0.5 O 3

shaozhen li (origen2003@126.com)
Wuhan polytechnic University
A. Rahman
University of Science and Technology of China
C. L. Ma
Suzhou University of Science and Technology
X. Zhao
Wuhan polytechnic University
Z. Y. Sun
Wuhan polytechnic University
M. F. Liu
Hubei Normal University
X. Z. Wang
Hubei Normal University
X. F. Xu
Hubei Polytechnic University
junming liu
Nanjing University

Research Article

Keywords:

Posted Date: February 24th, 2022

DOI: https://doi.org/10.21203/rs.3.rs-1237680/v1

Abstract

Bulk $Bi_{0.5}Sr_{0.5}Fe_{0.5}Cr_{0.5}O_3$ is a new compound comprising the R3c structure. The structural, magnetic, and exchange bias details are investigated. The material was in the paramagnetic state at room temperature. The field cooling H_{FC} acts on the sample resulting in the exchange bias H_{EB}. And the material is in a spontaneous polarization state, the exchange bias usually occurs at the boundary between ferromagnetic and antiferromagnetic states. The result shows that changing H_{FC} from 1T to 6T reduces the H_{EB} value by 16% at 2 K. Meanwhile, H_{EB} diminishes as the ferromagnetic layer thickens. The variation of t_{FM} with the change of H_{FC} leads to the tuning of H_{EB} by H_{FC} in bulk $Bi_{0.5}Sr_{0.5}Fe_{0.5}Cr_{0.5}O_3$. These effects are obviously different from the phenomenon seen in other oxide types.

Introduction

Researches show that exchange coupling occurs at the ferromagnetic (FM) and antiferromagnetic (AF) interface layers. When a magnetic field H is applied, once the sample temperature is below the AF layer Néel temperature, the FM layer exhibits unidirectional anisotropy because of the exchange coupling[1, 2]. As a result, the hysteresis loop shifts along the field axis. The strength of the shift is determined by the exchange bias (EB). Field H_{EB} can be affected by the magnitude of cooling field H_{FC}[3]. There are some EB effects in artificial material systems, for example, FM-AFM bilayers, FM-AFM superlattices, and topological-insulator /antiferromagnet containing ferromagnetic antiferromagnetic (FM-AFM) components [4–11].

Some progress has been made in the investigation of man-made EB structures. However, there are still some issues with the use of artificial structures that have been modified with various material phases. Mismatch between two material components with different sintering temperatures may result in ionic chaotically diffuse at the material interface; additionally, artificial EB materials require the assistance of static H cooling.The artificial EB usually benefits from field-cooling process. And when no static H is present, some special magnetic systems can exhibit spontaneous exchange bias (SEB). When the electric field can control the SEB effect, these materials can exhibit unidirectional anisotropy without external H, and the SEB effect will unavoidably be exploited in exchange bias (EB) devices. In recent years, investigations have demonstrated unusual zero-field-cooled (ZFC) EB and large SEB in a variety of systems, including $BiFeO_3$-$Bi_2Fe_4O_9$ nanocomposite, NiMnIn, Mn_2PtGa, $La_{1.5}Sr_{0.5}MnCoO_6$, $Pb_6Ni_9(TeO_6)_5$, $Y_{0.2}Ca_{0.8}MnO_3$, and $Bi_{10}Fe_6Ti_3O_{30}$ polycrystalline samples[12–18].

Materials with SEB effect should be investigated further to better understand the mechanism. Baettig and Spaldin performed first-principles calculations on the $BiFeO_3$–$BiCrO_3$ system[19]. A double-perovskite Bi_2FeCrO_6 with a long-range Fe^{3+}–Cr^{3+} order was hypothetically constructed, and a magnetic moment of 2 μB per formula unit and a polarization of 80 μC/cm^2 were predicted [19]. Experiments focused on the substituting effect of Cr ion for Fe ion on the physical properties of BFO. Kim et al. investigated the dielectric properties of 3mol % Cr doped BFO thin films synthesized by chemical solution deposition

technique. But in bulk, it is difficult to prepare, so $SrCrO_3$ and $Bi(Fe,Cr)O_3$ must be both prepared under high pressure[21]. Therefore, we investigate the $Bi_{0.5}Sr_{0.5}Fe_{0.5}Cr_{0.5}O_3$ system in search of stable perovskite phases that may exhibit some of the above-mentioned properties. The structure and magnetic properties of the new phase $Bi_{0.5}Sr_{0.5}Fe_{0.5}Cr_{0.5}O_3$ under ambient pressure are investigated. The results show that $Bi_{0.5}Sr_{0.5}Fe_{0.5}Cr_{0.5}O_3$ has the potential to be a new class material, which could help to expand the temperature range that can be measured.

Results

1. XRD patterns

Figure 1 depicts the XRD patterns of $Bi_{0.5}Sr_{0.5}Fe_{0.5}Cr_{0.5}O_3$ at 23°C. The diffraction data reveals the same structure with a hexagonal R3c unit cell, which is similar with $BiFeO_3$ previously reported[21]. Since Sr ionic has a smaller size than Ba and the ionic size of Cr is smaller than Fe, this leads to the lattice parameters change. To discuss the structural parameter changes, the structure was refined using Rietveld, and the data was fitted to the experimental pattern. The lattice parameters were refined using the high-resolution synchrotron XRD data shown in Table 1. It is found that the lattice parameters, both *a* and *c* decrease because Sr and Cr substitute Bi and Fe, respectively. The in-plane lattice parameter *a* is reduced to 0.557262 nm, and the out-of-plane lattice parameter *c* is reduced to 1.35006 nm. No additional reflections and impurities are detected in the room-temperature XRD data of bulk $Bi_{0.5}Sr_{0.5}Fe_{0.5}Cr_{0.5}O_3$.

Figure 2 illustrates the Fe 2p and Cr 2p XPS spectra of bulk $Bi_{0.5}Sr_{0.5}Fe_{0.5}Cr_{0.5}O_3$. Fe^{3+} ions have binding energies. Figure 2(a) shows the Cr 2p XPS spectrum. The energies 576.2 eV and 586.2 eV correspond to Cr $2p_{1/2}$ and Cr $2p_{3/2}$, respectively. It demonstrates that the Cr ions in BSFCO are mainly Cr^{3+}[23].The Fe $2p_{3/2}$ and Fe $2p_{1/2}$ peaks at about 711.7 eV, Fe $2p_{3/2}$ and 725.3 eV, and Fe $2p_{1/2}$ with a satellite at 719.6 eV[22–23]. Therefore, it can be deduced that the Fe ions in the bulk BSFCO are primarily Fe^{3+} in Fig. 2(b), with a few Fe^{2+} ions present to compensate for oxygen vacancies that cannot be determined.

2.The Mössbauer spectrum and magnetization of bulk BSFCO

Mössbauer data for bulk BSFCO samples at 300K(a)and 80K(b) are shown in Fig. 3(a) Mössbauer spectroscopy is used to demonstrate the bulk paramagnetic behavior at room temperature: the data show no magnetism. Mössbauer data at 300 K can be fitted to a doublet profile. It is a paramagnetic/antiferromagnetic material with an isomer shift of 0.16(0) mm/s, which is a property of the Fe^{3+} cation. The property of quadrupole splitting indicates the presence of a distorted octahedral environment, which agrees with bond distances refined from X-ray diffraction.

The low-temperature Mössbauer data in Fig. 3(b) show that the transition at 80 K is to a magnetically ordered or frozen state. The 80-K spectrum was fitted to a six-line magnetic profile (in green) and a double magnetic profile (in black). The double magnetic profile indicates that there is some paramagnetism at 80 K. The quadrupole interaction at 80 K is 0.40(7) mm/s. Meanwhile, the width of the spectrum at 80 K

is wider than that at 300 K. This is due to the fact that the hyperfine field of Fe is dispersed with 50% Cr^{3+} instead of Fe^{3+} [24].

ZFC-FC curves are measured to investigate the magnetization of bulk BSFCO at low temperatures as shown in Fig. 4. Figure 4 shows the magnetization curves of bulk BSFCO at zero field and cooling field at H = 1 T and T = 300 K. The bulk magnetic behavior of $Bi_{0.5}Sr_{0.5}Fe_{0.5}Cr_{0.5}O_3$ is revealed by magnetization measurements and plotted as a M-T curve. The ZFC and FC curves split around 130 K, while the FC curve (H = 1 T) has a plate-like peak and magnetization decreases rapidly below 25 K. Fitted by the Curie-Weiss law

$[\chi(T) = C/(T-\Theta_{CW})]$, which yields a Curie constant of 2.66 emu K/mol and a Weiss temperature Θ of -130 K. The negative Θ_{CW} suggests an antiferromagnetic coupling and T_N is about 25 K as evinced by the FC curve. The plate-like curve suggests the existence of competing interactions among its ferromagnetic property, antiferromagnetic property, and spin glass exit, consequently it may not be linked to spin glass-like freezing with long range order, but a transition to short range order.

3.M-H properties

To confirm these magnetic properties, the hysteresis loops of magnetization were collected from − 1 T to 1 T at 2 K after ZFC and FC under H = 1 T from 300 K, as shown in Fig. 5. The M-H loop under ZFC state is symmetric around zero, whereas the existence of exchange bias was proved by the shift of FC loops towards negative field. H_{EB} and H_C parameters are defined as $H_{EB} = (H_1 + H_2)/2$ and $H_C = -(H_1-H_2)/2$, respectively, where H_1 and H_2 are the left and right coercivity fields. H_{EB} was about 1150 Oe under the FC condition. H_C obtained from the FC loop is about 460 Oe and it is slightly higher than H_C obtained from ZFC (410 Oe). The different value results from the function of the exchange anisotropy.

It is shown in Fig. 6, with the reduction of H_{EB} and H_C by subsequent magnetization reversals, namely, the so-called training effect. This effect indicates that the exchange anisotropy slowly decreases. From the M-H loops (Fig. 6), it is observed that the ZFC magnetizations at 1 T, 3 T, and 5 T are much smaller than their FC counterparts. So FC can enlarge the content of the FM region and t_{FM}. The increase of t_{FM} under FC conditions reduces strain anisotropy, which arises from different magnetic states among the FM layer, the AF layer, and disordered spin glass; meanwhile, the strain anisotropy could cause the decrease of H_C.

Because H_{FC} can improve t_{FM}, we can deduce that changing H_{FC} can affect t_{FM} and the ratio of H_C^{FC} and H_{EB}^{FC}, as shown in Fig. 7. By connecting each data point, which represents the sample being cooled from 300 K to 2 K from 1 T to 1 T, the sample was cooled from 300 K to 2 K from 1 T to 1 T. Figure 7 shows a hysteresis loop. With an increase in H_{FC}, both H_C^{FC} and H_C^{FC} decrease. When H_{FC} increases from 1 T to 6 T, H_{EB} decreases by 16% at 2 K. It is not difficult to conclude from the above analysis that strain anisotropy could decrease because an increase in t_{FM} may result in a decrease in H_C^{FC}. To demonstrate the relationship between t_{FM} and H_{EB} in bulk BSCFO, the dependence of t_{FM} on H_{FC} must be confirmed.

From the M-H loop, the magnetization of the FM layers is almost saturated under an applied field of 1 T. M_{sat}, defined as $(M_{1T}\text{-}M_{-1T})/2$, is proportional to the volume fraction of the FM region. M_{sat} increases with H_{FC} when t_{FM} emerges, so the M_{sat}-H_{FC} curve plotted in Fig. 7 scales the variation of t_{FM} with H_{FC}. H_{EB} and $1/M_{sat}$ have a quasi-linear relationship, as illustrated in Fig. 8. As shown in Fig. 8, H_{EB} decreases as t_{FM} increases, which is consistent with the trend in exchange bias films. The result demonstrates the presence of FM coupling at the FM/AF interface in BSCFO. The AF coupling at the interface would result in a competition between the exchange energy and the Zeeman energy. It would weaken the relationship between H_{EB} and $1/t_{FM}$. This trend deviates from the linear prediction. It is worth noting that H_{FC} changes the thickness t_{AF} of the AF layer, which has an impact on H_{EB}.

This implies that the majority of the regions in the system are AF, but t_{FM} remains constant after sample fabrication without being affected by H_{FC}. The interfacial spins of FM and/or AF layers with H_{FC} will have an effect on H_{EB} change. The spontaneous FM and AF layers in BSCFO remain constant, allowing t_{FM} to be tuned after fabrication utilizing external forces. The mutual interactions of charge, spin, and lattice degrees of freedom in this bulk material can result in a delicate balance of different ground states. Magnetic field, electric field, laser light, pressure, and other forces can disrupt the equilibrium and cause it to transition to a new state.

Figure 9 illustrates schematic diagrams of the AFM/FM structure for bulk BSCFO at various magnetic fields. Since the FM increases as magnetic fields increase, some AFM structures can be tuned into FM structures. FM structure can be influenced with AFM by interfacial coupling, so the magnetization can be changed to a greater extent under a PM background, as shown in Fig. 9 (□□□□). It is identified from above that external fields have an effect on the interaction between the AF and FM layers. Furthermore, it benefits FM phase enhancement, as increasing H_{FC} can increase the ration of FM content and t_{FM} while decreasing H_{EB}. This indicates that, in the presence of certain external factors, the sensitivities of order parameters can be used to tune the exchange bias. Some recent studies suggest that short disorder is beneficial to FM clusters/microstructure in $La_{1.5}Sr_{0.5}CoMnO_6$ and Mn_2PtGa materials. The exchange anisotropic coupling of the embedded phase between FM and AFM layers has resulted in SEB. Thus, it's reasonable to assume that the SEB in bulk BSFCO is due to the coupling between the AFM layer, spin glass, and FM layer. To summarize, the analysis of exchange bias in these types of materials may lead to unusual events, which could aid in the creation of multifunctional spintronic devices.

Experiment

$Bi_{0.5}Sr_{0.5}Fe_{0.5}Cr_{0.5}O_3$ (BSFCO) bulk was prepared by solid reaction. High-purity $SrCO_3$, Bi_2O_3 (10% excess), Fe_2O_3, and Cr_2O_3 were intimately synthesized for 24 h, in stoichiometric quantities with solid reaction method under flowing nitrogen at 950°C and 1100°C. X-ray powder diffraction supplied the formation of a single perovskite type phase. Powder x-ray diffraction(XRD) data were collected on SmartLabSE. The data were analyzed by using the GSAS suite of Rietveld analysis programs. A superconducting quantum interference device magnetometer was employed to carry out magnetization

measurements. After undergoing zero field (ZFC) cooling and field (FC) cooling, measurements were conducted when the sample was heated from 5 K to 300 K under H = 1T. A magnetization loop was measured at 5 K. Mössbauer data were obtained using a conventional constant acceleration Mössbauer spectrometer incorporating a 25 mCi source of ^{57}Co in an Rh matrix. The valence states of Fe ions and Cr ions in bulk BSFCO were detected by the X-ray photoelectron spectroscopy (Al kα source, hν = 1.486 eV).

Declarations

Acknowledgements

Research was sponsored by the National Natural Science Foundation of China (11374147,12074111);Science and Technology Support Action Plan of 'Universities serve rural

References

1. A.Soumyanarayanan, M. Raju, A. L. Gonzalez Oyarce, A. K. C. Tan, Mi-Young Im, A. P. Petrović, Pin Ho, K. H. Khoo, M. Tran, C. K. Gan, F. Ernult and C. Panagopoulos, Tunable room-temperature magnetic skyrmions in Ir/Fe/Co/Pt multilayers, Nat. Mater. **16**, 898–904 (2017).
2. V. Skumryev, S. Stoyanov, Y. Zhang, G. Hadjipanayis, D.Givord and J. Nogués, Beating the superparamagnetic limit with exchange bias, Nature (London) **423**, 850–853 (2003).
3. F. M. Bai, G. Yu, Y. C. Wang, L. C. Jin, H. Z. Zeng, X. L. Tang, Z.Y. Zhong, and H. W. Zhang. Strong exchange bias with the (110)-oriented $BiFeO_3$ films, Appl. Phys. Lett. **101**, 092401:1–5 (2012) .
4. R. L. Rodrı´guez-Sua´ rez, L. H. Vilela-Lea˜o, T. Bueno, J. B. S. Mendes, P. Landeros, S. M. Rezende, and A. Azevedo. Tunable misalignment of ferromagnetic and antiferromagnetic easy axes in exchange biased bilayers, Appl. Phys. Lett. **100**, 242406–4 (2012).
5. T. Maity, S. Goswami, D. Bhattacharya, Roy, SuperspinS, Glass Mediated Giant Spontaneous Exchange Bias in a Nanocomposite of $BiFeO_3$-$Bi_2Fe_4O_9$, Phys. Rev. Lett. **110**, 107201–2 (2013).
6. A. K. Nayak, M. Nicklas, S. Chadov, C. Shekhar, Y. Skourski, J. Winterlik, and C. Felser. Large Zero-Field Cooled Exchange-Bias in Bulk Mn_2PtGa, Phys. Rev. Lett. **110**, 127204:1–4 (2013).
7. N. Kanazawa, Y. Onose, T. Arima, D. Okuyama, K. Ohoyama, S. Wakimoto,K. Kakurai, S. Ishiwata, and Y. Tokura. Large topological Hall effect in a short-period helimagnet MnGe, Phys. Rev. Lett. **106**, 156603:1–4 (2011).
8. S. Dong, Q. F. Zhang, S. J. Yunoki, J.-M. Liu, and Elbio Dagotto, Magnetic and orbital order in $(RMnO_3)_n/(AMnO_3)_{2n}$ superlattices studied via a double-exchange model with strain, Phys. Rev. B **86**, 205121:1–10 (2012).
9. M. Ye, W. Li, S. Y. Zhu, Y. Takeda, Y. Saitoh, J. J. Wang, H. Pan, M. Nurmamat, K. Sumida, F. H. Ji, Z. Liu, H. F. Yang, Z. T. Liu, D. W. Shen, A. Kimura, S. Qiao, X. M. Xie, Carrier-mediated ferromagnetism in the magnetic topological insulator Cr-doped $(Sb,Bi)_2Te_3$, Nat. Commun. **6**, 8913:1–8 (2015).

10. L. G. Wang, C. M. Zhu, Z. M. Tian, H. Luo, S. L. Yuan. Negative magnetization and zero-feld cooled exchange bias effect in $Co_{0.8}Cu_{0.2}Cr_2O_4$ ceramics, Appl. Phy. Lett. **107**, 152406 (2015).
11. M. Gruyters, Spin-Glass-Like Behavior in CoO Nanoparticles and the Origin of Exchange Bias in Layered CoO Ferromagnet Structures, Phys. Rev. Lett. **95**, 077204:1–4 (2005) ;
12. T. Maity, S. Goswami, Bhattacharya, D. Roy, S. Superspin, Glass Mediated Giant Spontaneous Exchange Bias in a Nanocomposite of $LiFeO_3$-$Bi_2Fe_4O_9$, Phys. Rev. Lett. **110**, 107201:1–4 (2013).
13. B. M. Wang, Y. Liu, P Ren, B. Xia, K. B. Ruan, J. B. Yi, J. Ding, X. G. Li, L. Wang, Large Exchange Bias after Zero-Field Cooling from an unmagnetized State, Phys. Rev. Lett. **106**, 077203:1–4 (2011) .
14. A. K. Nayak, M. Nicklas, S. Chadov, C. Shekhar, Y. Skourski, J. Winterlik, and C. Felser. Large Zero-Field Cooled Exchange-Bias in Bulk Mn_2PtGa, Phys. Rev. Lett. **110**, 127204:1–4 (2013).
15. J. K.Murthy, and A. Venimadhav, Giant zero feld cooled spontaneous exchange bias effect in phase separated $La_{1.5}Sr_{0.5}CoMnO_6$, Appl. Phys. Lett. **103**, 252410:1–4 (2013) .
16. B. Koteswararao, T. Chakrabarty, T. Basu, B. K. Hazra, P. V. Srinivasarao, P. L. Paulose and S. Srinath, Large spontaneous exchange bias in a weak ferromagnet $Pb_6Ni_9(TeO6)_5$, Sci. Rep. **5**, 16480:1–7 (2017).
17. T. Qian, G. Li, T. Zhang, T. F. Zhou, X. Q. Xiang, X. W. Kang, and X. G. Li, Exchange bias tuned by cooling field in phase separated $Y_{0.2}Ca_{0.8}MnO_3$, Appl. Phys. Lett. **90**, 012503:1–4 (2007).
18. Y. Huang, G. Wang, S. Sun, J. Wang, R. Peng, Y. Lin, X Zhai, Z Fu, Y Lu, Observation of Exchange Anisotropy in Single-Phase Layer-Structured Oxides with Long Periods, Sci. Rep. **5**, 15261:1–10 (2015).
19. P. Baettig, C. Ederer, and N. A. Spaldin, First principles study of the multiferroics $BiFeO_3$, Bi_2FeCrO_6, and $BiCrO_3$: Structure, polarization, and magnetic ordering temperature, Phys. Rev. B **72**, 214105:1–8 (2005).
20. D. H. Kim, H. N. Lee, M. Varela, and H. M. Christen, Antiferroelectricity in multiferroic $BiCrO_3$ epitaxial films, Appl. Phys. Lett. **89**, 162904:1–3 (2006).
21. L. Ortega-San-Martin, A. J. Williams, A. S.. and J. Paul Attfifield, Frustrated Orders in the Perovskite $(Bi_{0.5}Sr_{0.5})CrO_3$, Chem. Mater. **21**, 2436–2441 (2009).
22. P. Mills and J. L. Sullivan, A study of the core level electrons in iron and its three oxides by means of X-ray photoelectron spectroscopy, J. Phys. D **16**, 723–732 (1983) .
23. J. F. Moudler, W. F. Stickle, P. E. Sobol, and K. D. Bomben, *Handbook of X-Ray Photoelectron Spectroscopy* Perkin-Elmer, Eden Prairie, MN, (1992), pp. 77–81.
24. M. R. Suchomel, C. I. Thomas, M. Allix, M. J. Rosseinsky, and A. M. Fogg, High pressure bulk synthesis and characterization of the predicted multiferroic $Bi(Fe_{1/2}Cr_{1/2})O_3$, Appl. Phys. Lett. **90**, 112909:1–4 (2007).

Tables

TABLE I. Refined structural parameters of $Bi_{0.5}Sr_{0.5}Fe_{0.5}Cr_{0.5}O_3$ from powder diffraction data collected at room temperature.

Atom (site)	x	y	z	Occ.
Bi1(6a)	0.00000	0.00000	-0.16667	0.5
Fe1(6a)	0.00000	0.00000	0.08383	0.5
Sr1(6a)	0.00000	0.00000	-0.16667	0.5
Cr1(6a)	0.00000	0.00000	0.08383	0.5
O1(18b)	0.50382	0.50011	0.83835	1
SP: R3c, a = 5.57262 , b = 5.57262, c = 13.65006				
Chi^2 = 1.877, R_{wp} = 5.97%, R_p = 4.58%				

Figures

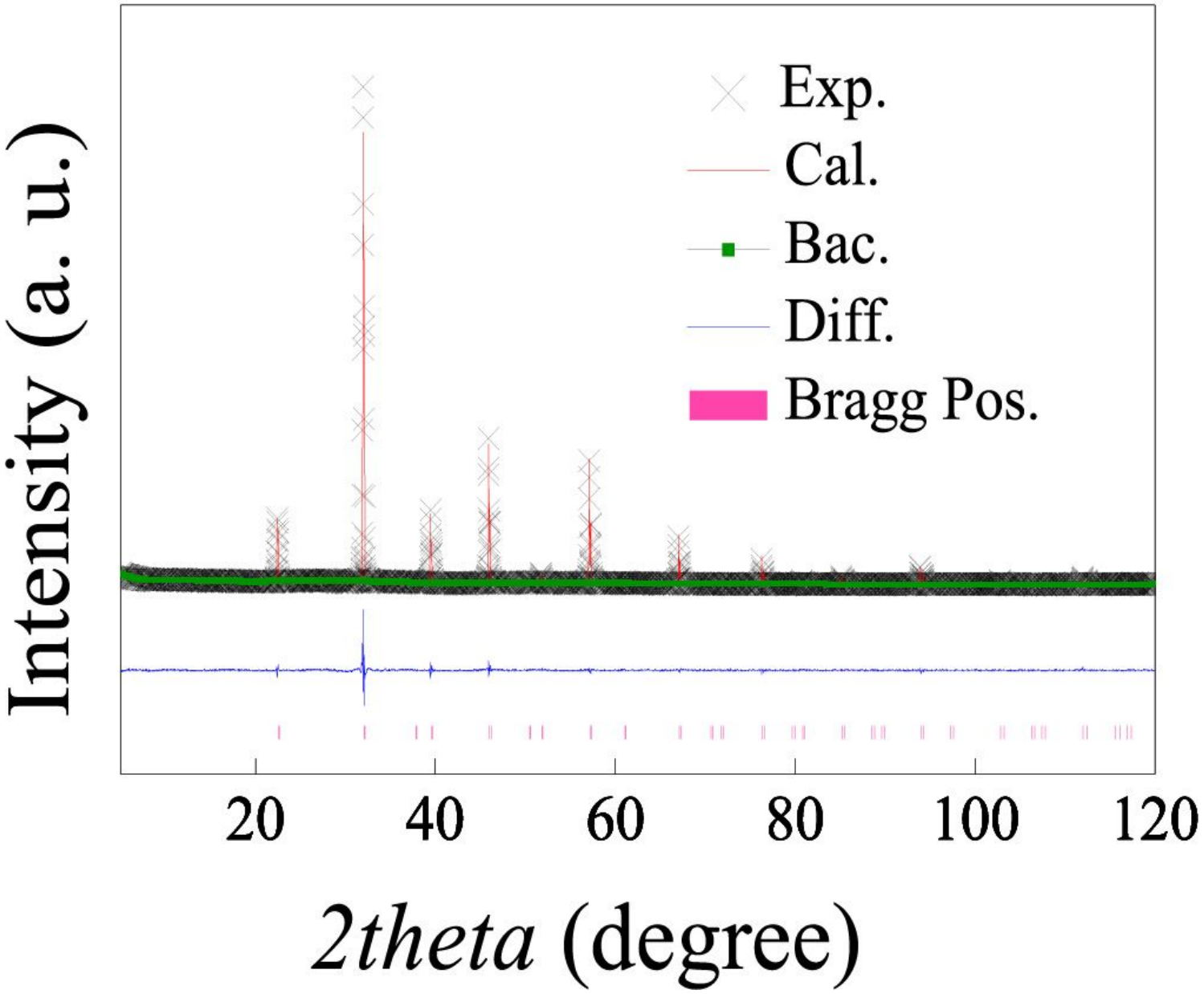

Figure 1

The room temperature X-ray diffraction patterns for BSFCO are shown. The refined structure diffraction data are observed together with the experimental data points using Rietveld refinement.

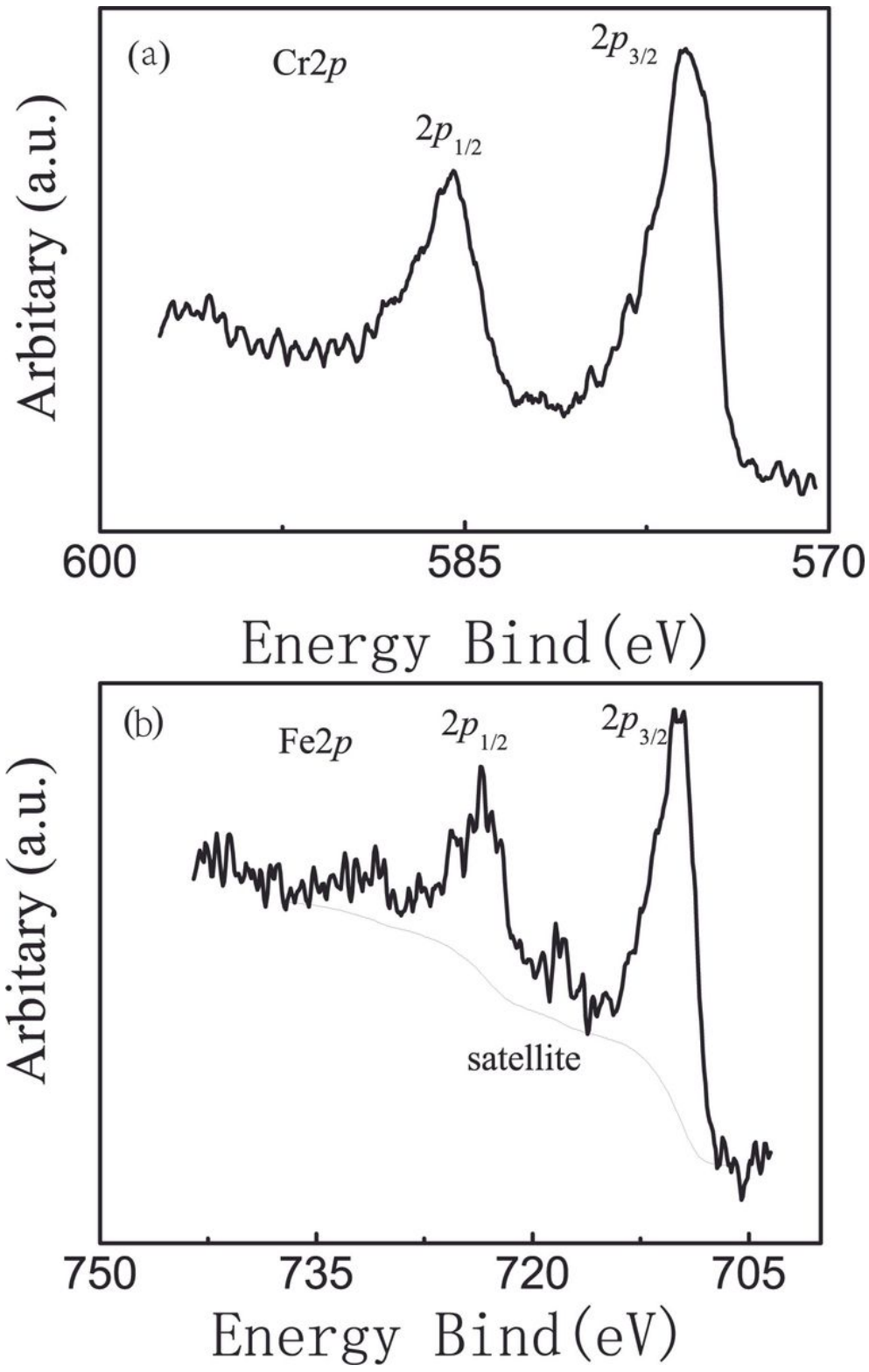

Figure 2

The core level XPS spectra for constituent elements in bulk BSCFO a) $Cr^{3+}$and b) for Fe^{3+}.

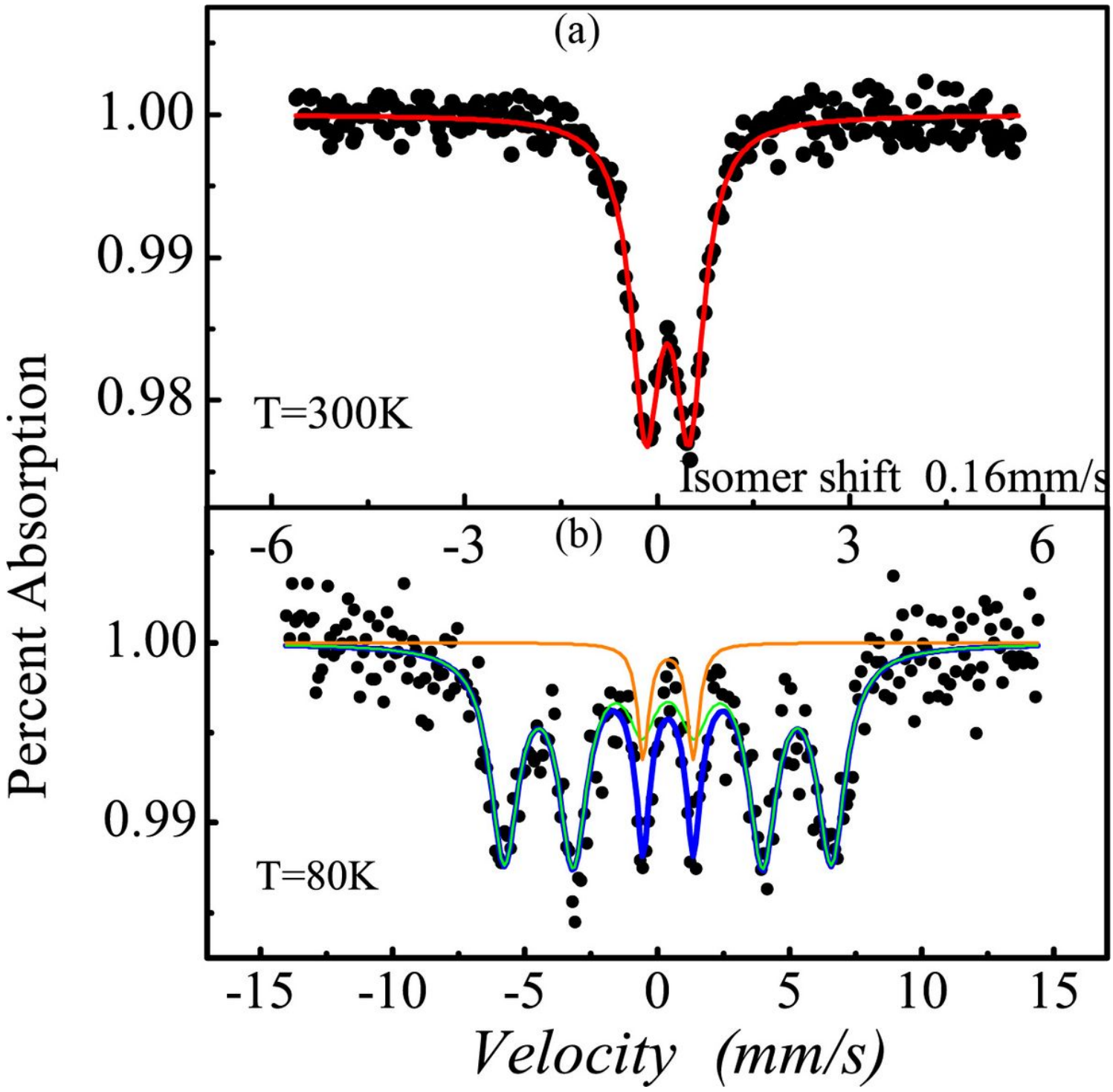

Figure 3

The Mössbauer data of bulk BSCFO at 300 K(a) and 80 K(b).

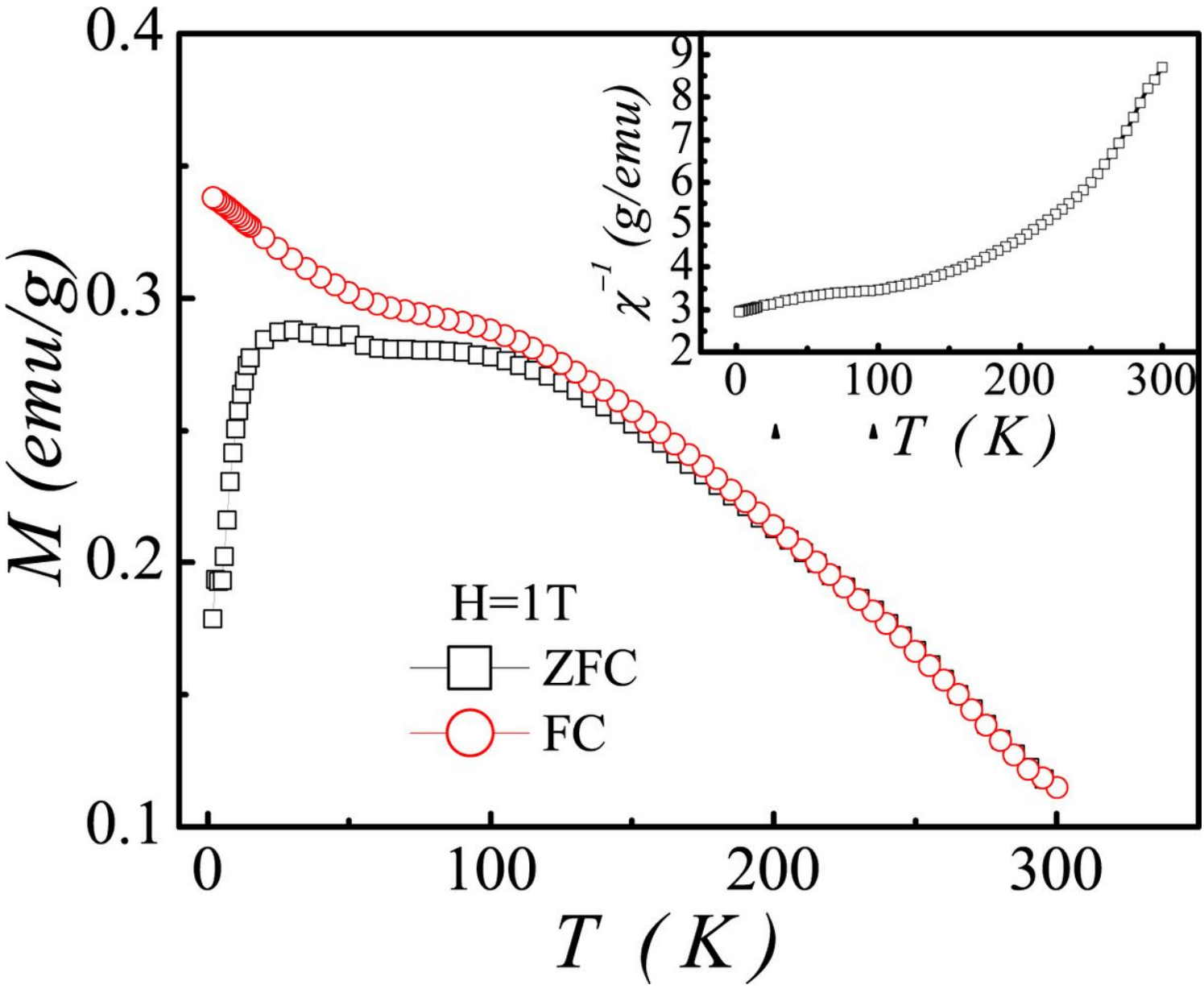

Figure 4

The ZFC and FC curve of BSCFO bulk; inset shows the Weiss law fit.

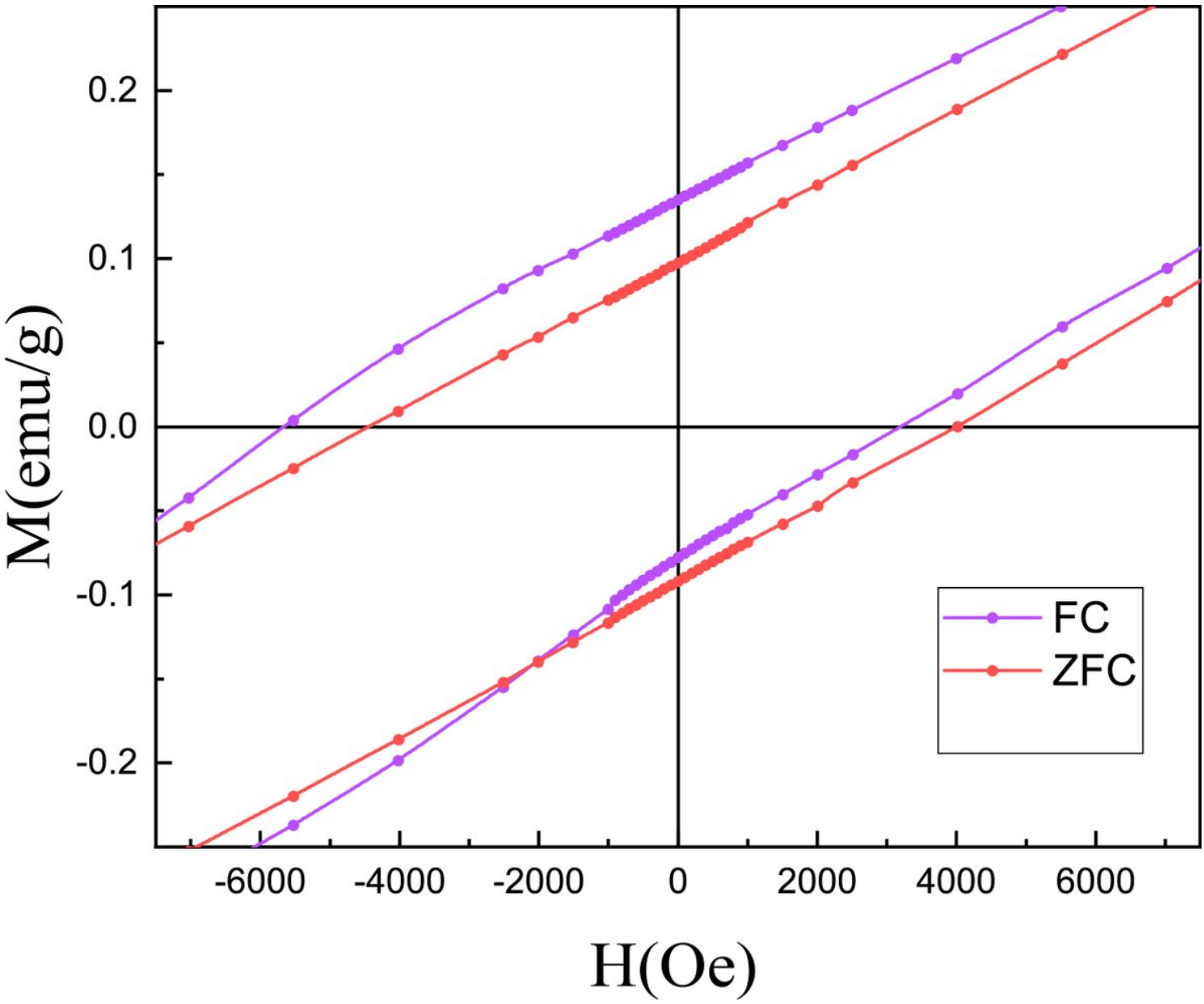

Figure 5

Hysteresis loops of magnetization at 2 K after ZFC and FC under *H* = 1 T from 300 K.

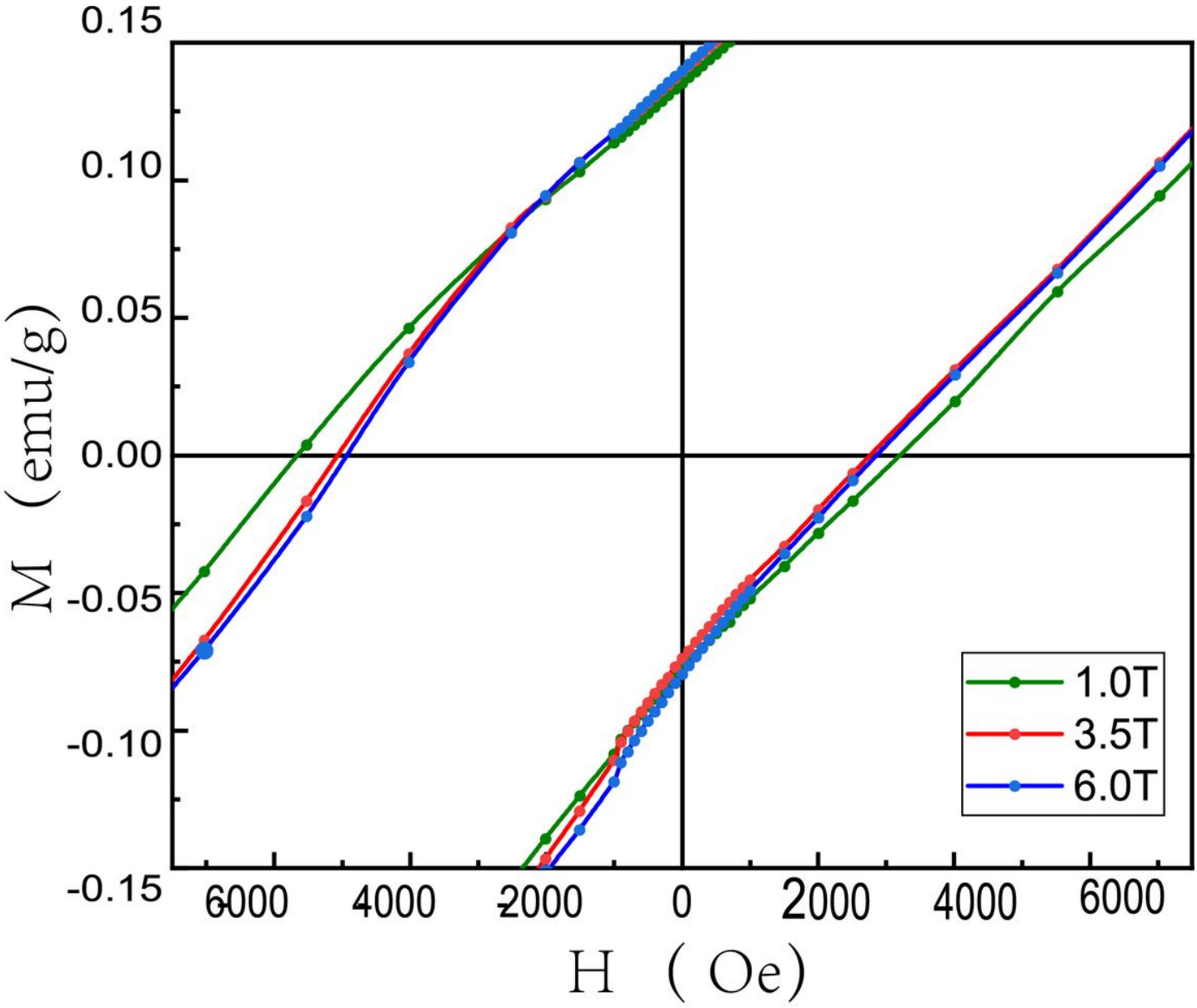

Figure 6

Hysteresis loops of magnetization at 2 K after FC under *H* = 1 T, 3 T, and 6 T.

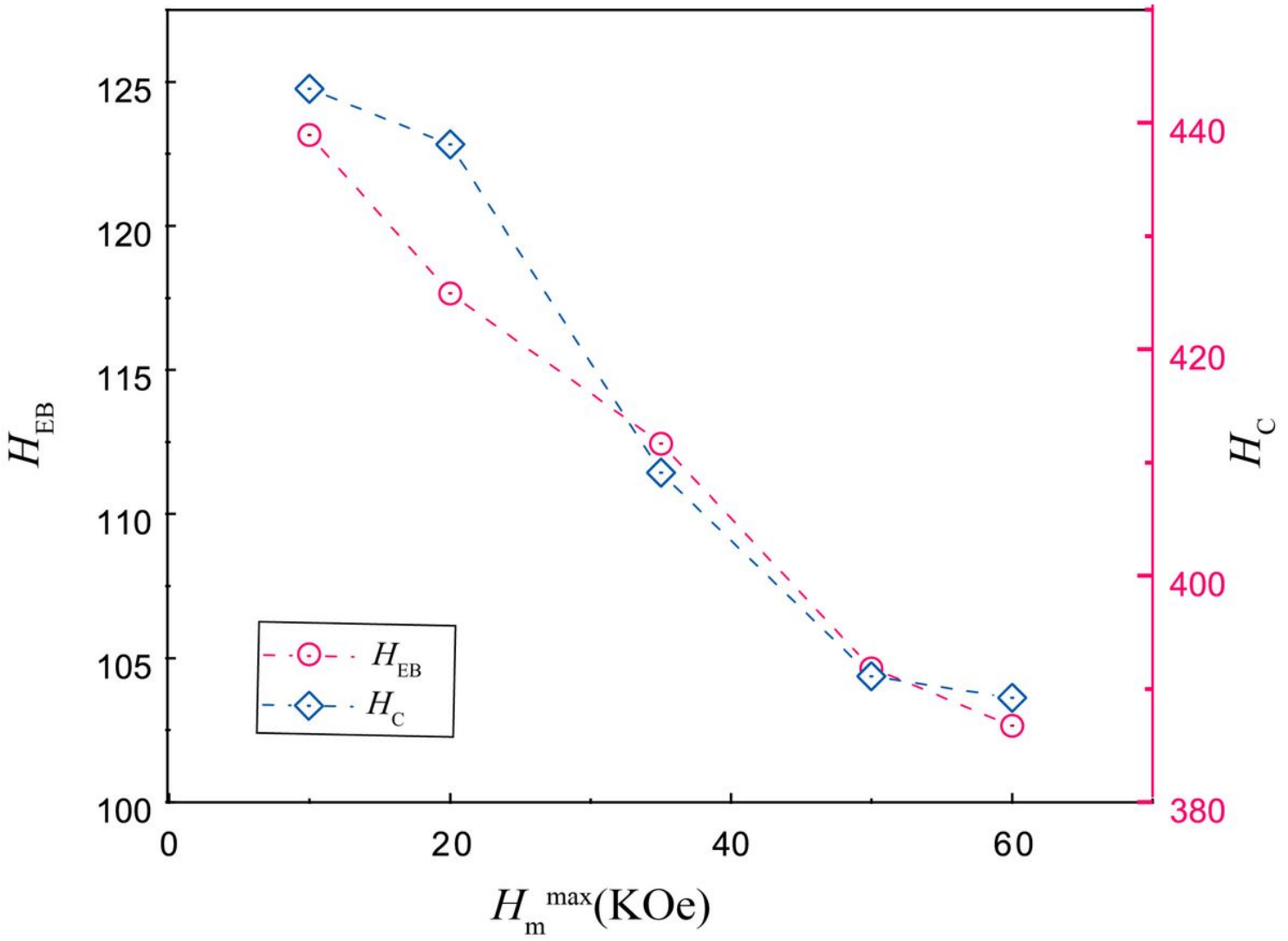

Figure 7

H_{FC} dependence of H_C^{FC} (right-hand axis) and H_{EB} (left-hand axis) at 2 K. H_C^{FC} and H_{EB} decrease linearly with H_{FC}. The lines are provided as a guide to the eye.

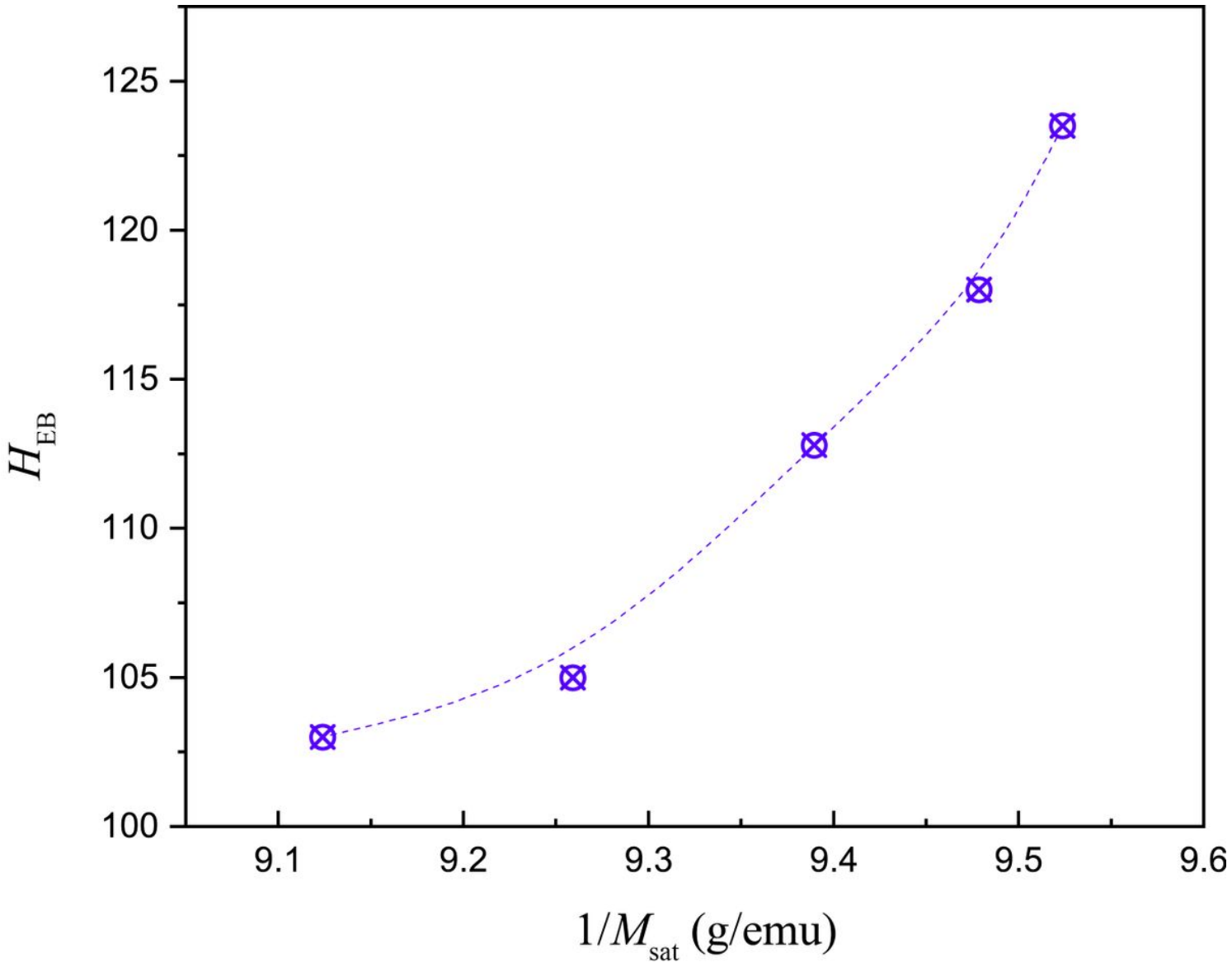

Figure 8

Linear relationship between H_{EB} and $1/M_{sat}$ at 2 K. Note that M_{sat} scales t_{FM}, indicating that the exchange bias in bulk BSFCO follows $H_{EB} \propto 1/t_{FM}$.

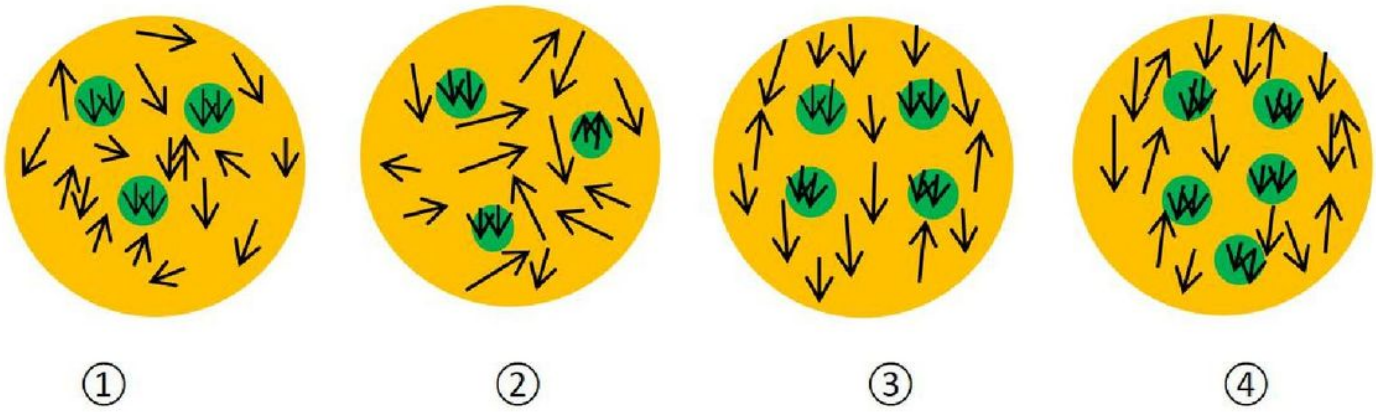

Figure 9

Schematic diagram of the AFM/FM core-shell structure for bulk BSCFO under different magnetic fields.

The datasets generated and/or analyzed during the current study are available in the [CSD Crystallographic data] repository, [Summary of Data - Deposition Number 2151932,

Compound Name:Data Block Name: data_BFSC_publ

Unit Cell Parameters: a 5.57262(5) b 5.57262 c 13.65006(10) R3c